A New Method for Quantitative Evaluation of Perforation Damage in Sandstone Targets

Aijun Zhang[1(✉)] and Hao Liang[2]

[1] China Oilfield Services Limited Well Tech, Haikou 570300, Hainan, China
274824362@qq.com
[2] CNOOC China Limited, Hainan Branch, Haikou 570300, Hainan, China

Abstract. High speed metal jet in perforating operation penetrates the oil and gas reservoir and forms a compaction zone near the hole, which causes damage to the porosity and permeability of the reservoir and seriously affects the productivity of oil and gas wells. At present, the traditional experimental methods are mainly used to evaluate the perforation damage. These methods are only a general qualitative and quantitative evaluation of single perforation technology or perforation target compaction zone damage, but they do not analyze and evaluate the damage characteristics and damage degree of sandstone target after perforation from point, line, surface, axial and radial perspectives of perforation channel, and have not compared the damage degree of sandstone target perforated by different perforation technology and charge type conditions. Therefore, a new method for quantitative evaluation of damage degree of sandstone target under different perforating technology or charge type is proposed, which can realize the multi-dimensional perforation damage characteristics of macro plane (point, line, surface) and along the axial and radial direction of perforating channel. Through the experimental study of four groups of perforating charges or perforating technology, the zonal characteristics of perforating target permeability zone are defined, and the quantitative evaluation of sandstone perforation compaction damage degree is realized. It is revealed that negative pressure perforation can reduce the damage rate and thickness of the compacted zone. There is a strong linear relationship between perforation depth and compaction zone area, perforation depth and average compaction thickness. The deeper the perforating charge penetrates, the greater the permeability damage rate of the compacted zone, and it shows logarithmic relationship. The new method has important engineering guiding significance for understanding the damage mechanism of perforated sandstone, quantitative evaluation of damage degree, improvement of perforating technology, optimization of perforating charge and suggestion of reducing perforation reservoir damage.

Keywords: sandstone target · perforation damage · core scanning · permeability · compaction

1 Introduction

Perforation is one of the important tasks in oil and gas field exploration and development. The efficiency of perforation directly affects the discovery of oil and gas fields, as well as the effectiveness of development and production, especially in low porosity and

B. Sun et al. (Eds.): DWOG-Hyd 2023, LNCE 472, pp. 198–211, 2024.
https://doi.org/10.1007/978-981-97-1309-7_19

permeability oil and gas fields [1–3]. During the perforation process, high-speed metal jets penetrate the oil and gas layer, causing significant damage to the rock structure around the perforation channel. This damage forms a "compaction damage zone" or "perforation damage zone" near the perforation hole [4]. As a result, rock porosity and permeability decrease, severely impacting the productivity of oil and gas wells.

To clarify the impact of perforation on reservoir damage, both domestic and foreign scholars have conducted a series of studies from experimental and theoretical perspectives. Pucknell et al. [4] employed various methods such as the mercury intrusion method, slice analysis, and radial flow permeability testing instrument to evaluate the porosity, particle size distribution in damaged areas, and permeability of Berey sandstone targets after perforation. Behrmann et al. [5, 6] conducted indoor flow testing experiments on perforated sandstone cores and confirmed that a low permeability area is not always present adjacent to the perforation channel. Saucier [7] and Feng et al. [8] confirmed the presence of compaction zones through visual observation of perforated targets cut along the channel. Rochon et al. [9] calculated the contribution of the fractured zone to the total skin effect of reservoir damage based on the analysis of the effective thickness and permeability changes of the fractured zone in perforated sandstone targets. Halleck et al. [10] studied the indentation hardness around the perforation channel and found that the damage gradually decreased from the perforation inlet to the end of the channel. Huang et al. [11], Li et al. [12], and Sun et al. [13] discovered that the physical property boundary between the compacted and uncompacted areas of the perforation target is relatively clear, and the porosity gradually increases from the outer edge of the compacted zone to the pore wall. This is mainly due to the compression and breakage of rock particles, resulting in particle microcracks and large pores. Juliane [14] used rock strength parameters to describe the damage caused by perforation in terms of the permeability of the perforation target and the degree of decrease in rock strength. Research has shown that the rock strength decreases as the distance from the perforation channel decreases. Overall, the current main method for evaluating perforation damage is to use traditional experimental methods such as mercury injection, electron microscopy, slice analysis, and naked eye observation to assess the damage of the perforation compaction zone. However, there has been no systematic analysis and evaluation of the damage characteristics and extent of sandstone targets after perforation from multiple perspectives such as point, line, and surface. Additionally, no comparison of the damage extent of sandstone targets under different perforation processes and bullet conditions has been conducted. Therefore, the author proposes a new method for the quantitative evaluation of perforation sandstone target damage using a core scanning system, which can provide macroscopic planar (point, line, plane) and axial and radial multidimensional perforation damage characteristics, as well as quantitative evaluation of sandstone target damage under different perforation processes or projectile conditions. This study holds significant theoretical and engineering significance for understanding the damage mechanism of perforated sandstone, quantitatively evaluating the extent of damage, improving the perforation process, and suggesting measures to reduce sandstone perforation damage.

2 Experiment of Sandstone Target Perforation Damage

2.1 Experimental Principles of Core Scanning System

The automatic core scanning system [15] is an instrument that utilizes steady-state airflow injection technology to determine the permeability of any point in a core sample. The core instrument of this system is a gas permeability probe, which is an automatic scanning measurement probe placed on a platform (Fig. 1). It enables axial and radial plane (point, line, plane) permeability scanning of perforated sandstone targets, providing information about the distribution changes in target permeability. Additionally, it can obtain parameters such as perforation damage morphology, area, and thickness from a macro perspective, serving as a basis for micro-CT experimental sampling for microdamage analysis. The probe consists of a measuring probe that is pressed onto the surface of the sample. Pressurized gas, typically nitrogen, is injected through a hole (Fig. 2) and disperses into the surrounding atmosphere in an approximately hemispherical shape through a limited gas volume of the sample. Based on the experimental principle, the steady-state method is employed to calculate the permeability of any measuring point on the core sample.

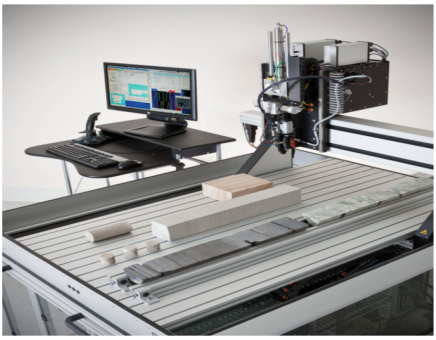

Fig. 1. Automatic scanning system with permeability probe

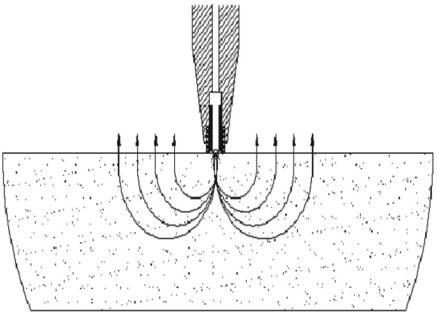

Fig. 2. Flow Principle of Probe Testing

The calculation formula for the apparent permeability of K_{apparent} in experimental testing is as follows:

$$K_{\text{apparent}} = 2Q\mu P_{\text{atm}} / \left[aG_{\text{o}} \left(P^2 - P_{atm}^2 \right) \right] \tag{1}$$

where, P is the injection pressure (Pa), P_{atm} is the atmospheric pressure (Pa), and Q is the volumetric flow rate (m^3/s) at atmospheric pressure, μ is the gas dynamic viscosity (Pa s), a is the internal top sealing radius (m), and G_o is the dimensionless geometric factor.

2.2 Experimental Sample Sampling Design

To observe the damage characteristics of the perforated sandstone target along the axis and radial direction of the perforation channel, the following preparation requirements for the perforated damage rock sample are suggested:

1) Splitting the perforation target: After the sandstone target is perforated, it should be split in half along the axial direction. One symmetrical half should be taken along the perforation channel for further analysis (Fig. 3).
2) Radial cutting: After the sandstone target is perforated, the perforation target should be cut radially at different axial positions, such as the entrance section, middle, and end, in the axial direction (Fig. 4).

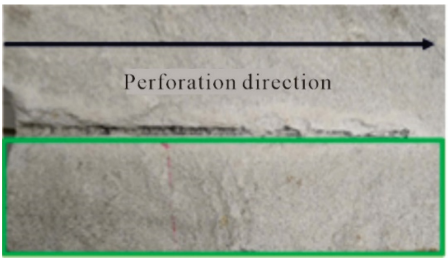

Fig. 3. Schematic diagram of axial section

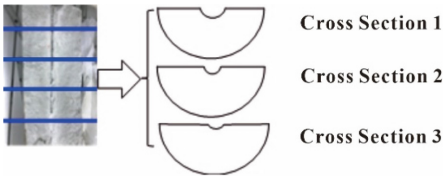

Fig. 4. Schematic diagram of radial profile

3 Analysis and Quantitative Evaluation of Damage Characteristics of Perforated Sandstone Targets

According to the perforation target damage evaluation method, the full core scanning system has the capability to perform continuous multi-point measurements of sandstone target permeability. It allows for quantitative characterization of sandstone target permeability at various points, lines, and surfaces.

According to the experimental principles and design ideas, a total of 21 sets of sandstone target perforation experiments were conducted. Table 1 presents four representative perforation experimental schemes.

3.1 Characteristics of Perforation Damage in Sandstone Targets

The automatic core scanning system is capable of measuring the permeability of perforated sandstone targets, lines, and surfaces. To achieve a qualitative and quantitative evaluation of the permeability distribution characteristics of sandstone target perforation damage, a clustering method was employed to analyze the zoning characteristics of the sandstone targets.

3.1.1 Principles of Cluster Analysis Methods

Clustering is indeed a data analysis technique that aims to group data points based on their similarity or distance of features. There are various clustering methods available, including hierarchical clustering and k-means clustering, which are commonly used in practice. In the context of evaluating the perforation damage zoning of sandstone targets based on their permeability distribution characteristics, the k-homogeneous clustering method is utilized.

Table 1. Perforation Experiment Plan

Number	Types of sandstone	Gun type - bullet type	Confining pressure MPa	Vacuum MPa
1	Beige sandstone	127 Guns -16 Hole Dense Ultra High Temperature Ammunition	5	0
2	Beige sandstone	127 Guns -16 Hole Dense High Temperature Deep Penetration Ammunition	5	0
3	Beige sandstone	127 Guns -16 Hole Dense High Temperature Deep Penetration Ammunition	30	10
4	Beige sandstone	127 Guns -16 Hole Dense Ultra High Temperature Perforating Ammo	25	5

The k-homogeneous clustering method leverages the concept of k-means clustering, which is an algorithm that partitions a given sample set into k subsets, forming k clusters. In this method, the permeability distribution data of the perforated sandstone targets are used as input. The algorithm aims to classify the data points into k homogeneous clusters, where each data point belongs to the cluster with the nearest centroid. It ensures that each sample is assigned to only one cluster and that the distance between each sample and the centroid of its assigned cluster is minimized.

1) **Method principle**

Given a set of n samples $X = \{x_1, x_2, \ldots xn\}$, each sample is represented by a feature vector with a dimension of m. The goal of k-means clustering is to divide n samples into k different classes or clusters, assuming $k < n$. k classes $G_1, G_2, \ldots G_k$ form a partition of sample set X, where $G_i \cap G_j = \Phi$, $\bigcup_{i=1}^{k} G_i = X \circ$Using C for partitioning, one partition corresponds to one clustering result.

K-means clustering can be attributed to the partitioning of sample set X or the selection of functions from samples to classes. The strategy of k-means clustering is to select the optimal partition or C * by minimizing the loss function. Firstly, the Euclidean distance squared is used as the distance $d(x_i, x_j)$ between samples.

$$\begin{aligned} d(x_i, x_j) &= \sum_{k=1}^{m} (x_{ki} - x_{kj})^2 \\ &= \| x_i - x_j \| \end{aligned} \tag{2}$$

The sum of the distances between the sample and the center of its class is defined as the loss function, which is:

$$W(C) = \sum_{l=1}^{k} \sum_{C(i)=l} \|x_i - \bar{x}_l\|^2 \tag{3}$$

where, $\bar{x}_l = (\bar{x}_{1l}, \bar{x}_{2l}, \cdots \bar{x}_{ml})^T$ is the mean or center of the l th class, $\bar{n}_l = \sum_{i=l}^{n} I(C(i) = l)$, $I(C(i) = l)$ is an indicator function with values of 1 or 0. The function $W(C)$, also known as energy, represents the degree to which samples in the same class are similar. Essentially, k-means clustering is about solving optimization problems:

$$\begin{aligned} C^* &= \arg\min_{C} W(C) \\ &= \arg\min_{l} \sum_{C(i)=l} \|x_i - \bar{x}_l\|^2 \end{aligned} \tag{4}$$

When similar samples are clustered together, the loss function value is minimized, and the optimization of this objective function can achieve the purpose of clustering.

2) **Basic steps of calculation**

Based on the basic principles of the clustering method mentioned above, the basic calculation process is shown in Fig. 5.

3.1.2 Characteristics of Sandstone Target Zoning

Based on the core scanning system testing, four sets of permeability data were collected at different locations of perforated sandstone targets. Corresponding permeability distribution cloud maps were generated, and the cluster analysis method [16–20] was applied to determine the zoning characteristics of the sandstone targets (Fig. 6). Analysis of the figure reveals distinct zoning patterns within the perforated sandstone target. The zoning characteristics of the perforated sandstone target can be observed from the figure. There is a clear high permeability zone, known as the fractured zone, within the perforation channel. Near the perforation channel, a clear low permeability zone, referred to as the compacted zone, is evident. Additionally, there may exist a transition zone between the fractured and compacted zones. The zone located farther away from the perforation channel represents the undisturbed zone or original zone. Significant differences in zoning characteristics are observed when comparing different perforation processes. For instance, in the case of negative pressure perforation, the transition zone may be masked or less pronounced compared to other perforation processes (Fig. 6e and Fig. 6g).

3.2 Quantitative Analysis of Perforation Damage

Based on the plane characteristics of perforation damage permeability, permeability variation curves were plotted along different radial directions (perpendicular to the perforation channel direction) of the perforation target channel. To facilitate a quantitative

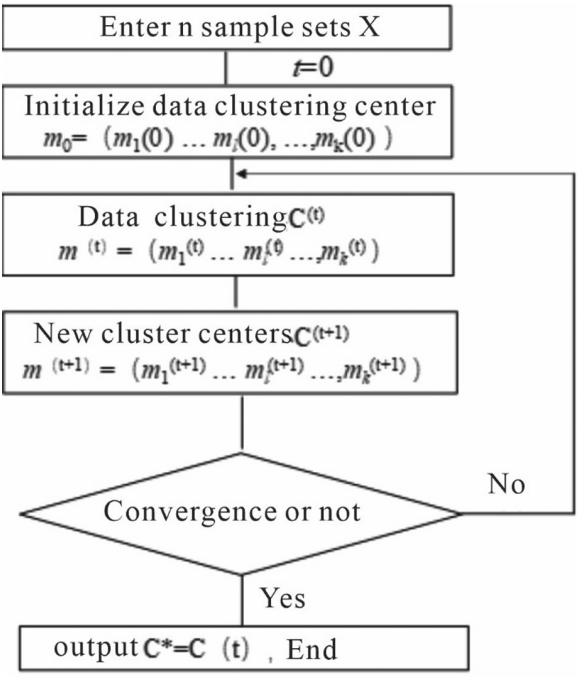

Fig. 5. Cluster analysis method calculation flowchart

comparison of perforation damage, a dimensionless comparative analysis of permeability was conducted, using the ratio of permeability (k) to the average permeability of the undisturbed zone. Figures 7, 8, 9 and 10 display the radial dimensionless permeability variation curves at different positions along the wellbore axis, considering different perforation processes or projectile conditions. The dimensionless permeability curves illustrate the relative changes in permeability compared to the average permeability of the undisturbed zone. Specifically, the permeability of the compacted zone is lower than that of the undisturbed zone, while the permeability of the fractured zone is higher. However, due to the variations in perforation processes and other conditions, each figure exhibits its own unique characteristics and differences. Overall, the dimensionless permeability of the compacted zone in Figs. 9 and 10 predominantly exceeds 0.5, indicating a relatively higher permeability in this zone. On the other hand, the permeability of the main body in Figs. 7 and 8 mostly falls below 0.5, suggesting a lower permeability compared to the undisturbed zone.

Based on a comprehensive analysis, it can be concluded that the perforation damage resulting from high confining pressure and negative pressure perforation processes (Figs. 9 and 10) is relatively lower than that caused by low confining pressure and non-negative pressure perforation processes (Figs. 6 and 7). This comparison is made by considering the dimensionless permeability curves and their respective characteristics. By employing dimensionless analysis and comparing the relative permeability changes, researchers can gain insights into the variation and severity of perforation damage under

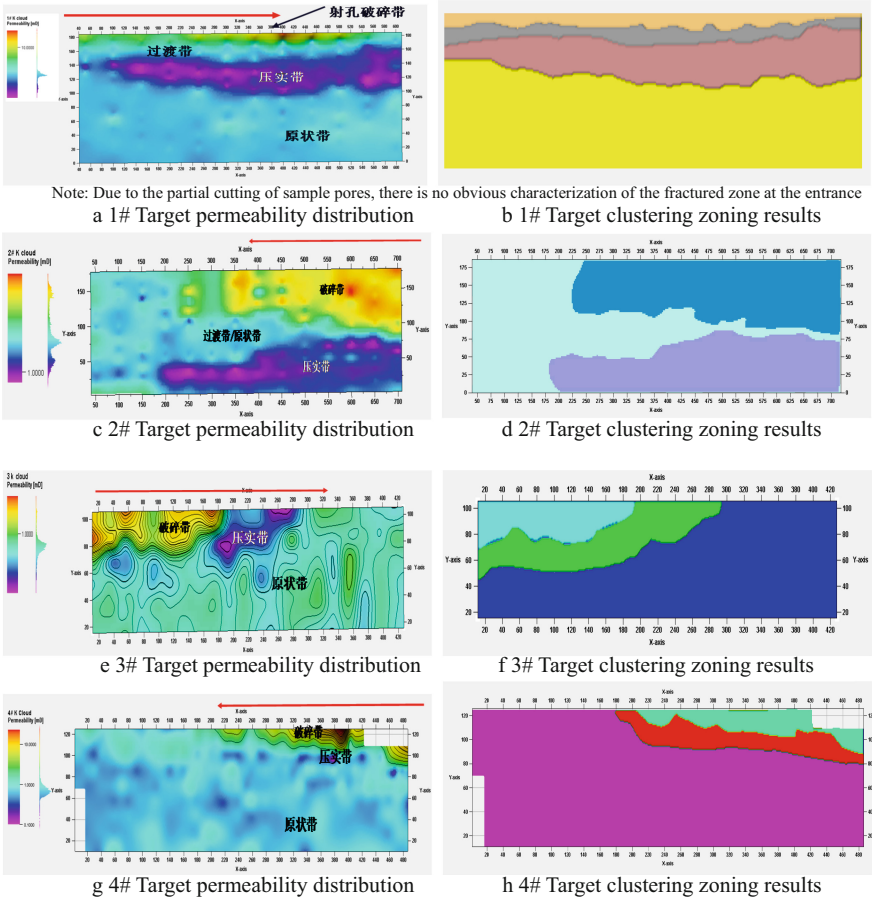

Note: Due to the partial cutting of sample pores, there is no obvious characterization of the fractured zone at the entrance

a 1# Target permeability distribution b 1# Target clustering zoning results

c 2# Target permeability distribution d 2# Target clustering zoning results

e 3# Target permeability distribution f 3# Target clustering zoning results

g 4# Target permeability distribution h 4# Target clustering zoning results

Note: The red arrow on the permeability distribution map from 1 # to 4 # represents the direction of the perforation channel;

There are obvious muddy bands in the sandstone target mixed with muddy bands in the graph

Fig. 6. Permeability distribution and clustering zoning characteristics of four sandstone targets

different conditions. This information is valuable for evaluating the effectiveness of various perforation processes and optimizing wellbore stimulation strategies.

The combination of clustering and zoning results with the radial dimensionless permeability curve results at different positions along the perforation axis has led to the generation of a comparison table of macroscopic parameters for perforation damage in different sandstone targets (Table 2). Upon examining the table, several observations can be made. One notable finding is that the permeability damage rate in the compaction zone of Target 3# is the lowest, measuring only 12%. Target 4# follows with a relatively low damage rate. This suggests that high negative pressure perforation leads to lower damage rates. Furthermore, deep penetration projectiles can generate deeper penetration distances, but they also cause more damage. This indicates a trade-off between penetration depth and damage severity. Additionally, under the same effective stress conditions,

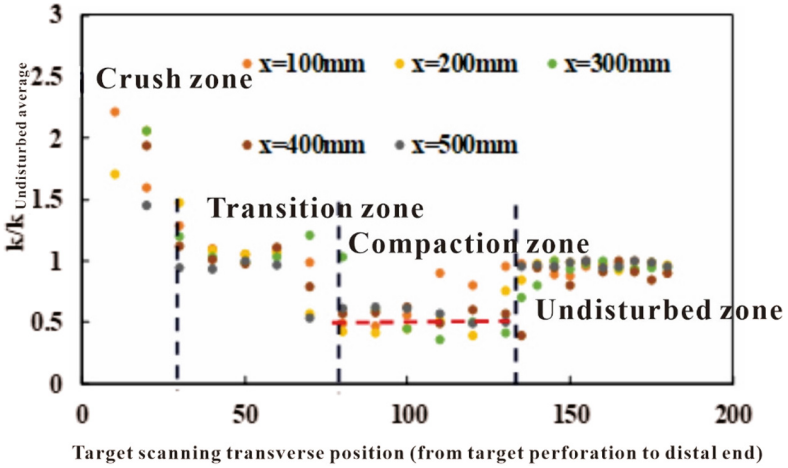

Fig. 7. 1# Target dimensionless permeability change curve

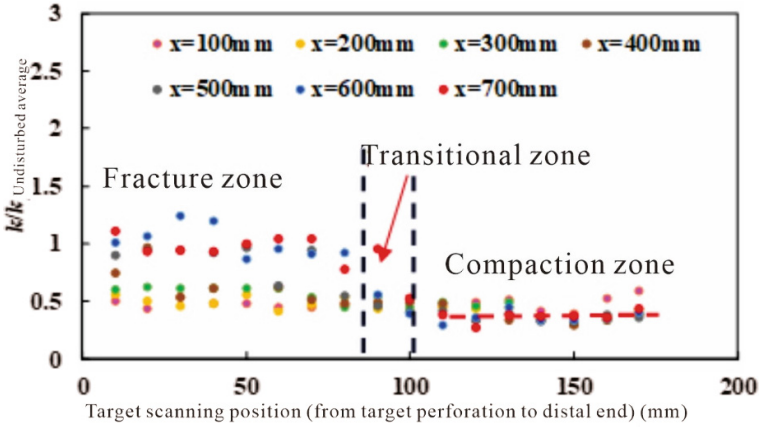

Fig. 8. 2# Target dimensionless permeability change curve

it is observed that the perforation damage caused by high-density perforating charges is lower than that caused by low-density perforating charges. This implies that the density of the perforating charges influences the extent of perforation damage. The comparison table provides a concise summary of the macroscopic parameters of perforation damage for different sandstone targets, allowing for a quick assessment of the relative damage rates and the impact of various perforation parameters. This information can aid in the selection and optimization of perforation processes and projectile types to minimize damage and enhance wellbore stimulation efficiency.

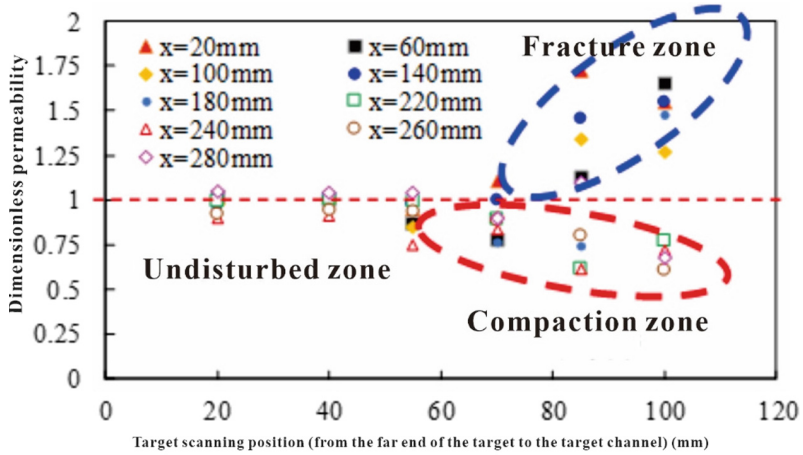

Fig. 9. 3# Target dimensionless permeability change curve

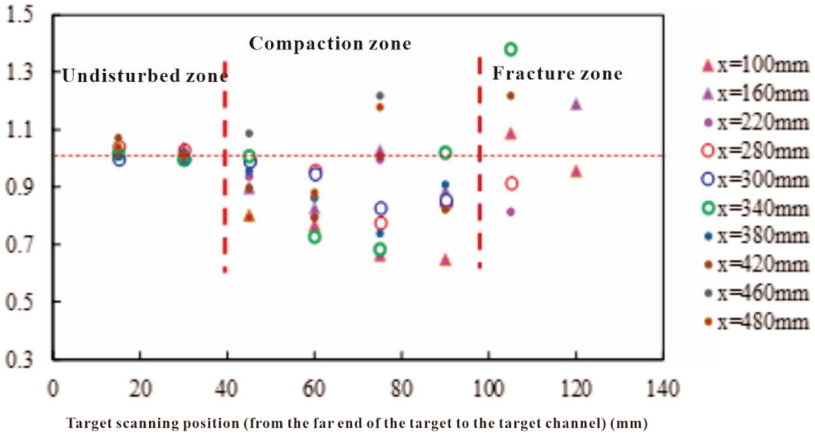

Fig. 10. 3# Target dimensionless permeability change curve

4 Analysis of Damage Law of Sandstone Target Under Different Perforating Bombs/Processes

Based on the comprehensive comparative analysis conducted on 12 sets of perforation sandstone targets and 7 types of perforation projectiles under different experimental conditions, the following key findings were observed regarding the quantitative evaluation of perforation sandstone target damage:

1) The compaction damage area of the high hole density (40 holes/m) perforation target was found to be smaller than that of the low hole density (16 holes/m) target (as shown in Fig. 10). This difference can be attributed to the inverse relationship between hole

Table 2. Comparison of perforation area parameters for different perforation targets

Target number	Bullet type	Confining pressure condition MPa	Vacuum MPa	Penetration depth mm	Crushing zone range	Transition zone range	Range of compaction zone Thickness of compaction zone	1-k/k_{raw}*100 Compaction damage rate, %
1#	127 guns -16 hole density Ultra-high temperature projectile	5	0	612	About 15 mm	About 40 mm	About 45 mm 44.53 mm	44
2#	127 guns -16 hole density High temperature deep penetration projectile	5	0	>800	About 88 mm	About 30 mm	About 66 mm 79.95	63
3#	127 guns -40 hole density DQ Deep penetration projectile	30	10	460	About 21 mm	/	About 17 mm 17.1 mm	12
4#	127 guns -16 hole density Ultra high temperature perforating charge	25	5	170	About 30 mm	/	About 42 mm 40.1 mm	32

density and the energy of the perforation projectile. Higher hole density results in lower projectile energy, leading to reduced compaction damage.

2) A strong linear relationship was observed between perforation penetration depth and both the compaction zone area and the average compaction thickness (with the exception of two blue outliers) (as depicted in Fig. 11 and Fig. 12). This linear relationship implies that as the penetration depth of the perforation increases, the resulting compaction zone area and average compaction thickness also increase proportionally.

3) The analysis revealed that there is a logarithmic relationship between the penetration depth of the perforating bullet and the permeability damage rate of the compacted zone (as shown in Fig. 13). As the penetration depth increases, the permeability damage rate of the compacted zone also increases. Notably, this increase follows a logarithmic pattern, indicating that the rate of increase slows down as the penetration depth continues to rise.

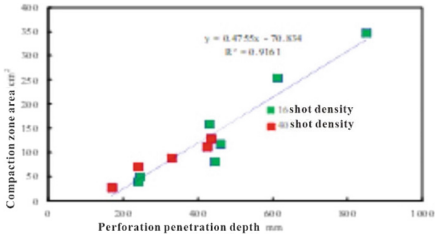

Fig. 11. Relationship between perforation penetration depth and compaction zone area

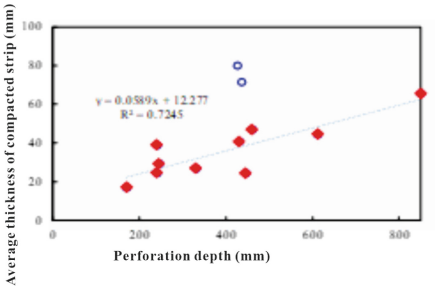

Fig. 12. Relationship between Hole Penetration Depth and Average Compaction Zone Thickness

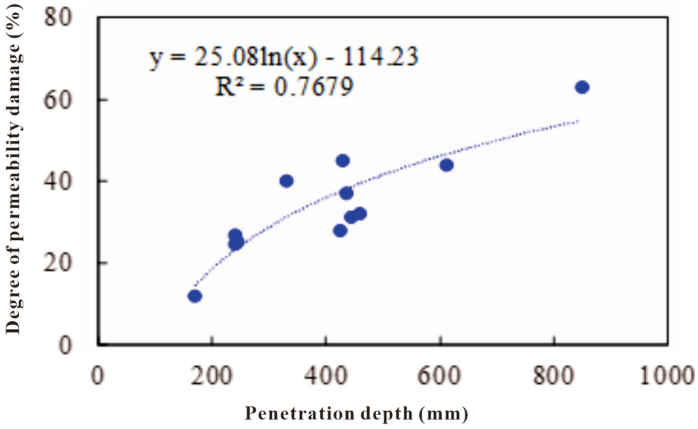

Fig. 13. Relationship between penetration depth of perforation target and permeability damage rate of compacted zone

From Fig. 11, Fig. 12 and Fig. 13, it can be seen that as the penetration depth of the perforation projectile increases, the amplitude of the increase in the damage rate of the compaction zone weakens. However, as the penetration depth of the perforation increases, the area and thickness of the compaction zone increase. Therefore, based on the results of the perforation damage experiment, there is a certain degree of contradiction between the depth of the perforation, the permeability damage rate of the

compaction zone, the area of the compaction zone, and the thickness of the rock zone, Implementing the coordination relationship between perforation depth, compaction area and thickness, compaction permeability damage rate, and production capacity under different perforation charges/process conditions has important guiding significance for the release of production capacity in low permeability and ultra-low permeability oil and gas reservoirs.

5 Conclusion

1) A new method has been proposed for quantitatively evaluating the perforation damage of sandstone targets using an automatic core scanning system. This method achieves quantitative evaluation of the macroscopic plane (point, line, plane), axial and radial multi-dimensional characteristics of perforation damage, as well as the damage degree of sandstone targets.
2) The core scanning system and clustering method were utilized to clarify the permeability distribution characteristics of four types of perforation targets. In the negative pressure perforation sandstone target, three distinct zones are observed: fractured zone, compacted zone, and undisturbed zone. In the non-negative pressure perforated sandstone target, four zones can be identified: fractured zone, transitional zone, compacted zone, and undisturbed zone.
3) Negative pressure reduces the damage rate and thickness of the perforation compaction zone. The perforation damage of high-density perforation charges is lower compared to low-density perforation charges.
4) The compaction damage parameters of four types of perforating charges and two types of perforating processes (low confining pressure - no negative pressure and high confining pressure - negative pressure) were compared. The results indicate that the 127-40 DQ deep penetration compaction exhibits the lowest thickness and compaction damage rate.
5) There is a certain degree of contradictory relationship between perforation depth, compaction permeability damage rate, compaction zone area/rock zone thickness, and production capacity. Specifically, there is a strong linear relationship between perforation depth and compaction zone area, as well as between perforation penetration depth and average compaction thickness. However, increasing the perforation depth leads to higher compaction zone permeability damage rate, following a logarithmic relationship. It is recommended to implement a coordinated relationship between perforation depth, compaction area and thickness, compaction permeability damage rate, and production capacity under different perforation charges/process conditions in future studies.

References

1. Niu, C., Zhang, Y.: Perforation Technology for Oil and Gas Well Completion, pp. 1–17. Petroleum Industry Press, Beijing (1994)
2. Niu, C.Q., Zhang, Y.J.: Perforation Technology For Oil and Gas Well Completion, pp. 1–17. Petroleum Industry Press, Beijing (1994)

3. Yuan, J.: Current situation and development of perforation technology in China. Logging Technol. **26**(5), 421–425 (2002)
4. Yuan, J.C.: On the development of perforating technology in China. Well Logging Technol. **26**(5), 421–425 (2002)
5. Tang, Y., Pan, Y., Zhu, Y.: Finite element numerical simulation study on non-Darcy flow perforation completion of gas wells. Acta Petrolei Sinica **13**(4), 85–96 (1992)
6. Tang, Y.L., Pan, Y.D., Zhu, Y.P.: Finite element numerical simulation research on non-darcy flow perforation completion of gas well. Acta Petrolei Sinica **13**(4), 85–96 (1992)
7. Pucknell, J.K., Behrmann, L.A., et al.: An investigation of the damaged zone created by perforating. Soc. Petrol. Eng. (1991)
8. Behrmann, L.A., et al.: Measurement of additional skin resulting from perforation damage. Paper SPE 22809 presented at the 1991 SPE Annual Technical Conference and Exhibition, Dallas, 6–9 October 1991
9. Behrmann, L.A.: Underbalance criteria for minimum perforation damage. SPE Drill. Complet. **11**(03), 173–177 (1996)
10. Saucier, R.J., Lands Jr., J.F.: A laboratory study of perforations in stressed formation rocks. J. Petrol. Technol. **30**(09) (1978)
11. Feng, Y., Pan, Y., Huang, Y.: Mechanism and evaluation criteria of perforation damage to production layers. Nat. Gas Ind. (06), 57–60+8–9 (1991)
12. Jean, R., Creusot, M.R., Feugas, D., et al.: Viscous fluids characterize the crushed zone. SPE Drill. Complet. **10**(03), 198–203 (1995)
13. Halleck, P.M., Robins, J., et al.: Mechanical damage caused by perforations may affect fracture breakdown. Soc. Petrol. Eng. (1998)
14. Huang, F., Sun, X., Luo, X., et al.: Experimental study on nuclear magnetic resonance in the perforated damage zone of Beilei sandstone. J. Beijing Univ. Technol. **S1**, 3–5 (1999)
15. Li, D., Tang, G., Sun, X., et al.: Research on perforated compaction zone. Pet. Explor. Dev. **27**(5), 112–114 (2000)
16. Sun, X., Liang, C., Wang, H., et al.: Research on the damage zone of shaped charge perforation. Logging Technol. (01), 33–36+100 (2006)
17. Heiland, J.C., Grove, B.M., Harvey, J.P., et al.: New fundamental insights into perforation-induced formation damage. Soc. Petrol. Eng. (2009)
18. Wei, Y.Q., Liu, G.M., Dong, Y.H.: Determinating effective porosity by the combination of three-dimensional laser scanning and gas displacement. Geol. Sci. Technol. Inf. **34**(04), 212–216 (2015)
19. Su, W.H.: Research on the theory and method of multi-index comprehensive evaluation. Xiamen University (2000)
20. Yang, X.B.: Research of key techniques in cluster analysis. Zhejiang University (2005)
21. Zhao, X., Liu, Y.T., Ding, Y., et al.: Fuzzy comprehensive recognition model of dominant water channels in offshore oilfield. Fault-Block Oil Gas Field **24**(01), 91–95 (2017)
22. Wang, S.L., Jiang, H.Q., Li, J.J., et al.: Determination of injection-production efficiency using ISODATA fuzzy clustering analysis method. Oil Drill. Prod. Technol. **33**(05), 61–64 (2011)
23. He, H., Peng, S.M., Huang, S.W., et al.: Flow units of conglomerate reservoir—an example from Badaowan formation in Midwest of District 2 in Karamay oilfield. Xinjiang Petrol. Geol. **30**(01), 96–99 (2009)